Bistable Conduction Electron Spin Resonance in Metallic Lithium Particles

Caroline Vigreux,[†] Laurent Binet,[‡] and Didier Gourier*[,§]

Ecole Nationale Supérieure de Chimie de Paris, Laboratoire de Chimie Appliquée de l'Etat Solide, UMR CNRS 7574, 11, rue Pierre et Marie Curie, 75231 Paris Cedex 05, France

Received: October 9, 1997; In Final Form: December 11, 1997

This paper reports the study by electron spin resonance (ESR) and electron nuclear double resonance (ENDOR) of lithium particles in Li_2O powders irradiated by 1-MeV electrons. The metallic lithium particles are characterized by a narrow ESR line ($\Delta B_{pp} = 0.013$ mT) due to conduction electrons and an ENDOR signal from ^{7}Li nuclei interacting with these electrons. The ESR of conduction electrons in lithium particles exhibits a bistable hysteresis of 0.18 mT width at $T = 4$ K due to steady-state bistable dynamic nuclear polarization by the Overhauser effect, in good agreement with theoretical predictions. The analysis of the bistable conduction electron spin resonance (BCESR) line shape showed the existence of two populations of particles differing by their electron spin relaxation times T_2 and characterized by a distribution of nuclear relaxation times.

I. Introduction

Bistable systems have attracted growing attention because of their potential application in data handling,[1] design of neural networks,[2] and stochastic resonance.[2−4] The bistability of the magnetic resonance of conduction electrons in solids constitutes an original memory effect of a transition in a two-level quantum system[5] formed by the spin states $m_s = \pm^1/_2$ of electrons in the conduction band of a solid. The transition between the two electron spin states interacting with an electromagnetic field B_1 of frequency ν in the microwave range is generally characterized by a single electron spin resonance (ESR) absorption line as shown in Figure 1a (dotted line). However, it was recently shown that the electron spin resonance may exhibit a bistable behavior corresponding to an ESR line bent at an angle of 45°, as shown in Figure 1a (full line), so that different ESR intensities are recorded according to the external field sweep direction.[5,6] This bistable conduction spin resonance (BCESR) results from a bistable dynamic nuclear polarization of nonzero nuclear spins interacting via hyperfine coupling with the conduction electrons. The dynamic nuclear polarization (DNP) occurs by the Overhauser effect[7] when the ESR transition of the conduction electrons is saturated. Indeed, all the electronic conductors containing nuclei with spins $I \neq 0$ are expected to be good candidates for BCESR provided that the following criterion is satisfied:[6,8]

$$I(I+1)NAf\gamma T_2 > \frac{12kT}{B_0} \qquad (1)$$

In this expression, N is the number of nuclear spins I interacting with each electron, A the hyperfine interaction for each nucleus, f the leakage factor ($0 \leq f \leq 1$) measuring the efficiency of the flip-flop process for nuclear polarization,[9] $\gamma = g\beta/h$ the electron gyromagnetic ratio, T_2 the spin−spin electron relaxation time, T the temperature, and B_0 the external magnetic field. If the external field is sufficiently high and the temperature sufficiently low, it is clear that inequality 1 will be satisfied in any solid with nonzero nuclear spins. This means that BCESR is a general property of conducting solids. Under given conditions of T and B_0, inequality 1 can also be satisfied if the term $I(I+1)NAf$ is high or T_2 is long. This is an essential requirement if BCESR is to be observed at room temperature and under weak magnetic fields. However, despite the generality of eq 1, BCESR was unambiguously observed only in gallium oxide β-Ga_2O_3 at room temperature[5] and in InP at liquid-helium temperature.[10] Therefore, the search for new compounds liable to exhibit such a bistable memory effect is of fundamental importance to validate the general character of the BCESR phenomenon. This bistable behavior implies nuclei with spins $I \neq 0$, but also a narrow CESR line width (long T_2) and an

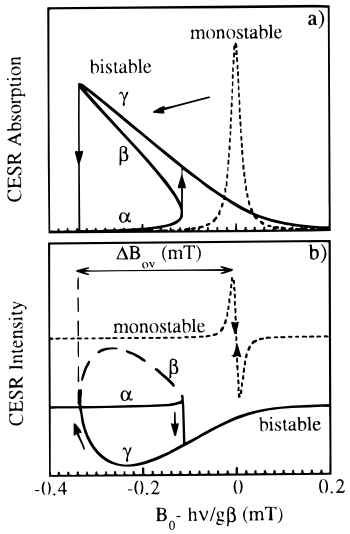

Figure 1. (a) Variations of the CESR absorption intensity for colloidal lithium particles at 4 K calculated from eqs 2−4. Parameters of the calculation are $T_1 \approx T_2 \approx 4.9 \times 10^{-7}$ s, $(\Delta B_{ov})_{max} \approx 0.4$ mT, microwave field $B_1 = 0.0019$ mT ($P = 0.16$ mW, discontinuous line), and $B_1 = 0.025$ mT ($P = 25$ mW, full line). (b) Theoretical CESR spectra for colloidal lithium particles at 4 K, at $P = 0.16$ mW (discontinuous line) and $P = 25$ mW (full line), calculated from eqs 2, 3, and 5 with the same parameters as in part a.

[†] E-mail: vigreux@ext.jussieu.fr.
[‡] E-mail: binetl@ext.jussieu.fr.
[§] E-mail: gourierd@ext.jussieu.fr.

S1089-5647(97)03283-5 CCC: $15.00
Published on Web 01/27/1998

intense dynamic nuclear polarization, corresponding to a high value of the term $I(I + 1)NAf$ in inequality 1. Metallic lithium particles exhibit CESR line widths in the range $10^{-3}-0.1$ mT [11] and a DNP corresponding to $I(I + 1)NAf$ on the order of 600 MHz.[12] They are thus promising candidates for the observation of the magnetic bistability of conduction electrons at liquid-helium temperature. In their pioneering work on the Overhauser effect in lithium particles, Gueron and Ryter noticed a dependence of the line shape on the direction of the field sweep that they did not explain.[13] The purpose of the present work is to demonstrate that the magnetic resonance of conduction electrons in colloidal lithium particles is intrinsically bistable and to show that the BCESR line shape is very sensitive to small variations of the relaxation times of the particles, as initially predicted.[6]

II. Experimental Part

Samples of 97 atom % pure Li_2O powder supplied by Aldrich were pressed into 7-mm diameter pellets. The pellets were annealed for 5 h at 900 °C in a vacuum (5×10^{-6} Torr) to eliminate LiOH and Li_2CO_3 and wrapped in a thick aluminum foil. They were then irradiated with 1-MeV electrons to a total dose of 10^{19} e^-/cm^2 from a van de Graaff accelerator under nitrogen atmosphere at 205 and 275 K. These temperatures were obtained by applying two different current intensities, 15 and 25 μA, and were measured with a thermocouple in contact with the sample surface. These experimental conditions correspond to those used by Vajda and Beuneu[14] and are known to give lithium particles with size smaller than the skin depth in the microwave range.

ESR experiments were performed with an X-band ESP 300e Bruker spectrometer equipped with a TE_{102} cavity. The microwave frequency is known with a precision of 10^{-5} GHz, which corresponds to an uncertainty on the ESR line position of 3.5×10^{-4} mT. ESR spectra above 100 K were obtained with a conventional nitrogen-flow system, while spectra below 100 K were recorded with a helium-flow cryostat from Oxford Instruments. The cavity constant relating the microwave power P and the microwave field B_1 is $K = P/B_1^2 = 4 \times 10^4$ mW mT^{-2} with the helium-flow cryostat.

Room-temperature electron nuclear double resonance (ENDOR) experiments were carried out with a Bruker cavity working in the TM_{110} mode and a 100-W ENI broad-band power amplifier. ENDOR spectra were detected with a 12.5-kHz modulation of the applied magnetic field. No ENDOR spectrum could be obtained with the usual frequency modulation of the radio frequency (rf) carrier.

III. Monostable CESR and ENDOR

The ESR spectrum of the sample irradiated at 205 K exhibits hyperfine lines of F^+ centers superimposed on a weak narrow line close to the free-electron g value ($g = 2.0023$). In the sample irradiated at 275 K, this narrow line at $g = 2.0023$ dominates (Figure 2a) while the hyperfine lines of the F^+ centers collapse into a weak and broad line. All these observations are consistent with the results of Vajda and Beuneu.[14] The narrow line was attributed to free electrons in metallic colloidal lithium particles. Actually, this narrow line in our samples has several features characteristic of conduction electron spin resonance. First, the line is motionally narrowed with an unsaturated peak-to-peak line width $\Delta B_{pp} = 0.013$ mT at $P = 0.16$ mW (Figure 2a) independent of the temperature, which means that the electron spin relaxation occurs mainly from collisions with defects or surfaces rather than from interactions with phonons. Second, the ESR intensity is also independent

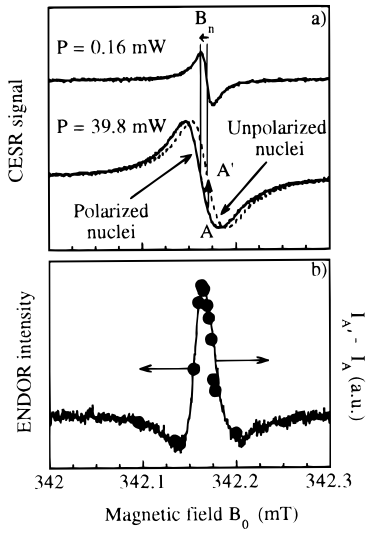

Figure 2. (a) Experimental CESR spectrum for colloidal lithium particles in Li_2O at $T = 295$ K and two microwave power values. The dotted line corresponds to the expected CESR spectrum at $P = 39.8$ mW ($B_1 = 0.028$ mT) without nuclear polarization. Sweeping time = 84 s. Modulation frequency = 12.5 kHz. Modulation amplitude = 5 μT. Microwave frequency $\nu \approx 9.58$ GHz. (b) Experimental ENDOR intensity versus magnetic field (full circles) compared to the difference between the two ESR signals at $P = 39.8$ mW (full line).

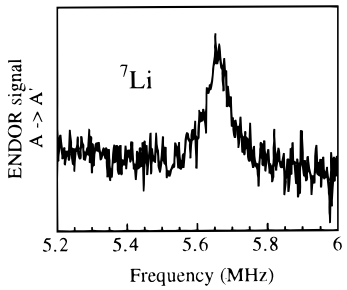

Figure 3. Room-temperature ^{7}Li ENDOR signal from colloidal lithium particles in Li_2O at $P = 39.8$ mW. Magnetic field setting is $B_0 = 342.17$ mT (point A in Figure 2a). The depolarization of nuclei by the external radio frequency field causes an increase in the ESR signal at the field setting A, which is responsible for the ENDOR signal. Sweeping time = 84 s. Modulation frequency = 12.5 kHz. Modulation amplitude = 5 μT.

of temperature, denoting the Pauli-type behavior of the magnetic susceptibility typical of conduction electrons. A definitive proof of the delocalized character of the electrons at the origin of the narrow line is supplied by ENDOR. Lithium has two isotopes (^{6}Li, $I = 1$, 7.5% natural abundance; ^{7}Li, $I = {}^3/_2$, 92.5% natural abundance). The ENDOR response of lithium nuclei in metallic lithium particles was first observed by Feher and Isaacson in Li−LiF systems.[15] The origin of the ENDOR response is the following. When the CESR line is saturated, the DNP caused by the Overhauser effect creates a magnetic field B_n that shifts the CESR line to low fields. Then when the NMR transitions of the nuclei interacting with the conduction electrons are saturated by the rf field, the nuclear field vanishes and the CESR line shifts back to its original position. Thus, a variation of CESR intensity at a given field setting B_0 is recorded, which constitutes the ENDOR response. When the narrow ESR line of a sample irradiated at 275 K is saturated at $P = 39.8$ mW, a small shift of $7.2 \times 10^{-3} \pm 0.7 \times 10^{-3}$ mT to low fields is observed (Figure 2a), which is consistent with the existence of a nuclear field B_n due to the DNP of lithium nuclei. Figure 3 shows the room-temperature ENDOR signal from the same

sample observed at $B_0 = 342.17$ mT. A line peaking at the nuclear frequency $\nu_n = 5.66$ MHz is observed, corresponding to the nuclear g factor $g_n = h\nu_n/(\beta_n B_0) = 2.17$ of ^{7}Li nuclei. To verify that the ENDOR response in electron-irradiated Li_2O originates from nuclear depolarization according to the mechanism described by Feher and Isaacson, the ENDOR intensity was plotted as a function of the field setting B_0 (full circles in Figure 2b). The uncertainty of the intensity is given by the size of the circles. The full line in Figure 2b corresponds to the intensity difference $I_{A'} - I_A$ between the actual ESR spectrum saturated at $P = 39.8$ mW (full line in Figure 2a) and the spectrum calculated with zero nuclear polarization (dotted line in Figure 2a). The uncertainties of the width and position of the calculated ENDOR intensity resulting from the uncertainties of the positions of the spectra of Figure 2a are 5×10^{-4} mT and 8×10^{-4} mT, respectively. The good agreement between the intensity of the ENDOR response and the ESR intensity difference $I_{A'} - I_A$ versus B_0 means that the ENDOR spectrum is really the result of the depolarization of lithium nuclei by the saturating rf field. This conclusively confirms that the electron spins at the origin of the narrow ESR signal in irradiated Li_2O originates from conduction electrons in metallic lithium particles.

IV. Bistable Conduction Electron Spin Resonance (BCESR)

(a) Background. The nuclear field B_n created by Overhauser effect[7] is generally much stronger than the nuclear field $B_n^0 = I(I+1)NA\nu_n/(3kTg\beta)$ resulting from the thermal polarization of the nuclear spins. It was previously shown[6] that the nuclear field B_n can be bistable if eq 1 is satisfied. In that case, B_n exhibits two different stable values for the same external field value B_0 according to the B_0-field sweep direction. The nuclear magnetic field B_n is given by the following equation:[5]

$$B_n = (\Delta B_{ov})_{max} \frac{\gamma^2 T_1 T_2 B_1^{\,2}}{1 + \gamma^2 T_1 T_2 B_1^{\,2} + \gamma^2 T_2^{\,2}[B_0 + B_n - h\nu/(g\beta)]^2} \quad (2)$$

which can exhibit up to three real solutions labeled B_n^α, B_n^β, and B_n^γ in increasing order, depending on the different parameters contained. In this expression $(\Delta B_{ov})_{max}$ represents the highest nuclear field achievable under given field B_0 and temperature T and is expressed by

$$(\Delta B_{ov})_{max} = \frac{I(I+1)NAfB_0}{3kT} \quad (3)$$

The other parameters of eq 2 are the electron spin−lattice and spin−spin relaxation times, respectively T_1 and T_2, the electron g factor, and the microwave field B_1. The solutions B_n^α, B_n^β, and B_n^γ represent the steady-state values of the nuclear field. B_n^α and B_n^γ correspond to the two stable states obtained respectively upon increasing and decreasing sweeps of B_0, while the intermediate value B_n^β corresponds to an unstable state. The ESR absorption I_{abs} is proportional to the saturation factor s of the transition and is given by[5]

$$I_{abs} \propto s = \frac{\gamma^2 T_1 T_2 B_1^{\,2}}{1 + \gamma^2 T_1 T_2 B_1^{\,2} + \gamma^2 T_2^{\,2}[B_0 + B_n - h\nu/(g\beta)]^2} \quad (4)$$

Consequently, under saturation conditions, the ESR absorption becomes itself bistable (full line in Figure 1a), since the resonance condition of the conduction electron spins is transformed into $h\nu = g\beta(B_0 + B_n)$ to take into account the bistable nuclear field B_n acting on the electrons. The nuclear field is negligible ($B_n \ll |B_0 - h\nu/(g\beta)|$) when the saturation is weak, and the ESR absorption is monostable (dotted line in Figure 1a) as usually encountered in ESR. The actual ESR intensity I_{ESR} corresponds to the derivative of the absorption with respect to the external field B_0 and is derived from the usual Bloch equations[16] in which the nuclear field B_n is added to the external field B_0 [5] so that

$$I_{ESR} = -I_0 \frac{(\gamma T_2)^3 B_1 [B_0 + B_n - h\nu/(g\beta)]}{\{1 + \gamma^2 T_1 T_2 B_1^{\,2} + \gamma^2 T_2^{\,2}[B_0 + B_n - h\nu/(g\beta)]^2\}^2} \quad (5)$$

where I_0 is a constant depending on both the spectrometer and the sample through the spin concentration and the electron spin polarization at thermal equilibrium.

Figure 1b shows the BCESR spectra expected from eq 5 for conduction electrons in lithium particles with parameters that will be determined below. The dotted line represents the common monostable spectrum with Lorentzian line shape, which is obtained at weak saturation (low microwave power) when the nuclear field B_n in eq 5 is negligibly small. When the microwave power is increased, the nuclear field becomes significant and a distortion as well as a hysteresis of the CESR spectrum according to the field sweep direction is predicted by simulation (full line in Figure 1b). The spectrum under increasing B_0 is computed by inserting the solution B_n^α of eq 2 into eq 5, while the spectrum under decreasing field is obtained with the solution B_n^γ. Moreover, the theoretical spectrum corresponding to the unstable state B_n^β (dashed line in Figure 1b) can also be calculated though it is not observable. The singularity indicated by the vertical line in the spectrum (Figure 1b) under decreasing sweep occurs at a field B_0 where the resonance condition $B_0 + B_n^\gamma = h\nu/(g\beta)$ is achieved.[5] Thus, the shift $\Delta B_{ov} = h\nu/(g\beta) - B_0$ of the singularity with respect to the resonance field $h\nu/(g\beta)$ at weak saturation is a direct measurement of the nuclear field B_n^γ at resonance.

(b) Experimental Results for Lithium Particles. The experimental BCESR spectra of conduction electrons in lithium particles in electron-irradiated Li_2O were recorded at $T = 4$ K (Figure 4). The magnetic field sweep rate was 2.4 mT min^{-1}, slow enough to ensure a steady-state nuclear polarization at each field value. At low microwave power ($P = 20$ μW), the CESR spectrum is independent of the field sweep direction and has the usual Lorentzian line shape. At higher microwave power, the CESR spectrum exhibits a hysteresis according to the field sweep direction of about 0.18 mT at $P = 25$ mW. To simulate the experimental BCESR spectra with eqs 2 and 5, we need an estimation of the electron spin relaxation times T_1 and T_2 and of the quantity $I(I+1)NAf$ in eq 3. These parameters can be obtained from the variation of the Overhauser shift ΔB_{ov} as a function of the microwave power P. Owing to the long sweep times required by the long nuclear relaxation time (on the order of 10 s at 4 K [17]) to maintain steady-state conditions, the Overhauser shifts were measured at $T = 19$ K. At this temperature, the steady-state conditions can be approached with faster sweep rates because of the decrease of the nuclear relaxation time. The Overhauser shifts versus the microwave power at $T = 19$ K is plotted in Figure 5. The experimental points fit the theoretical expression[12,18]

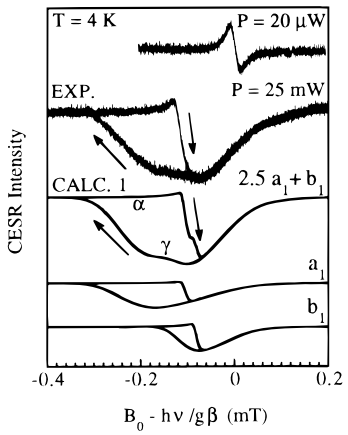

Figure 4. Experimental and calculated BCESR spectra for colloidal lithium particles in irradiated Li_2O at $T = 4$ K and $P = 25$ mW. The unsaturated spectrum at $B_1 = 0.007$ mT ($P = 20$ μW) is shown at the top right of the figure. The calculation (CALC 1) is performed from eqs 2, 3, 5, and 10 and includes two populations A and B for the particles, with Gaussian distributions of $I(I + 1)NAf$ and with parameters given in Table 1. The two spectra a_1 and b_1 represent the individual contributions of populations A and B to the total calculated CESR spectrum CALC 1. The other parameters of the simulation are $T_1 \approx T_2 \approx 4.9 \times 10^{-7}$ s and $B_1 = 0.025$ mT.

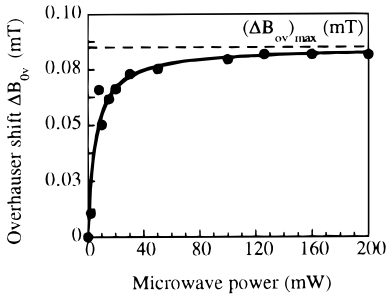

Figure 5. Experimental Overhauser shift ΔB_{ov} versus microwave power at $T = 19$ K. The full line corresponds to the simulation from eq 6 with $(\Delta B_{ov})_{max} = 0.085$ mT and $K/(\gamma^2 T_1 T_2) = 5.5$ mW.

$$\Delta B_{ov} = (\Delta B_{ov})_{max} \frac{P}{P + a} \tag{6}$$

with $(\Delta B_{ov})_{max} = 0.085$ mT and $a = K/(\gamma^2 T_1 T_2) = 5.5$ mW. Taking into account the fact that the condition $T_1 = T_2$ for motionally narrowed ESR lines in conductors is fulfilled, we derive from the value of $K/(\gamma^2 T_1 T_2)$ the following estimate of the electron spin relaxation times:

$$T_1 \approx T_2 \approx 4.9 \times 10^{-7} \text{ s} \tag{7}$$

This value is in relatively good agreement with that deduced from the unsaturated line width $\Delta B_{pp} = 0.019$ mT, which gives $T_1 \approx T_2 \approx 2/(\gamma\sqrt{3}\Delta B_{pp}) \approx 3.5 \times 10^{-7}$ s. With the experimental value of $(\Delta B_{ov})_{max}$ at 19 K, we obtain from eq 3

$$I(I + 1)NAf = 300 \text{ MHz} \tag{8}$$

However, steady-state conditions were not completely achieved for the Overhauser shift measurements at 19 K so that the value is probably slightly underestimated at this temperature. Therefore, the value $I(I + 1)NAf = 300$ MHz must be considered only as a rough estimate and a starting point for the simulation of the CESR spectra at 4 K, especially since the leakage factor f may itself depend on temperature.

The spectra at $T = 4$ K and $P = 25$ mW under increasing and decreasing field sweeps calculated from eqs 2, 3, and 5 and with the values of the material parameters given by eqs 7 and 8 are represented by the full lines in Figure 1b. It can be seen that, despite the uncertainties of the values of T_1, T_2, and $I(I + 1)NAf$, the agreement with the experimental spectra in Figure 4 is fairly good. In particular, the overall line shapes, Overhauser shift, and hysteresis width are correctly predicted. Thus, the hysteresis of the magnetic resonance of conduction electrons from lithium particules in Li_2O actually results from an intrinsic bistability of the steady-state polarization of lithium nuclear spins. However, some important features in the experimental spectra are not predicted by the calculation. More precisely, the slope on the left side of the experimental spectrum under decreasing field sweep and the discontinuity of the experimental spectrum under increasing field sweep are less steep than in the calculated spectra. This suggests a distribution of material parameters. Besides, a shoulder appears at the bottom of the experimental spectrum under decreasing field. This indicates the existence of two distinct populations of particles, hereafter referred to as A and B populations respectively, the first one with strong Overhauser shifts giving the major contribution to the CESR intensity and the second one with smaller Overhauser shifts responsible for the small shoulder in the decreasing field spectrum. The Overhauser shift corresponds to the nuclear field B_n^{γ} in the γ state at resonance. From expression 2 of the nuclear field B_n, we suggest a bimodal distribution of g factors as a first explanation for the shoulder. Population A with higher g factors would resonate at low fields, giving rise to the most shifted part of the CESR spectrum, while population B with smaller g factors would be responsible for the shoulder at higher fields. However, this explanation appears very unlikely, since it would imply a splitting of the unsaturated CESR line, which is not observed. Moreover, we were unable to simulate the CESR spectrum with a distribution of g factors. Two possibilities remain to account for a double distribution of Overhauser shifts. (i) First, the particles can be characterized by a bimodal distribution of leakage factor f, which controls the maximum Overhauser shift $(\Delta B_{ov})_{max}$ in eq 3. In that case this would reveal a distribution of nuclear relaxation times. (ii) The second possibility is a bimodal distribution of electron spin relaxation times T_1 and T_2. In fact, the electron spin relaxation times and the leakage factor are not independent. As a matter of fact, the leakage factor f is defined by

$$f = \frac{\nu_x}{\nu_x + \nu_n'} \tag{9}$$

where the electron−nucleus cross-relaxation frequency ν_x is related to the electron spin relaxation time T_1 by $\nu_x \approx [A/(h\nu)]^2 (1/T_1)$.[19] The other parameter ν_n' in eq 9 is the nuclear relaxation frequency corresponding to all the nuclear relaxation mechanisms different from the electron−nucleus cross-relaxation. Nothing is known about the behavior of ν_n' in our sample, and besides, this parameter may be submitted to more or less broad distributions that can partly disconnect the behavior of the electron spin relaxation times from that of the leakage factor. Therefore, in a first approximation, we can treat the electron spin relaxation times T_1 and T_2 as independent of the leakage factor f. This procedure allows us not only to reduce the number of adjustable parameters but also to study separately the effects of distributions of each parameter.

To test the hypothesis of a bimodal distribution of leakage factor (calculation 1), each population was characterized by a

TABLE 1: Parameters of the Gaussian Distributions Characterizing Populations A and B[a]

	populations					
	CALC 1		CALC 2		CALC 3	
parameters	A	B	A	B	A	B
$\langle I(I+1)NAf\rangle$ (MHz)	240	120	240	240	240	240
$\sigma_{I(I+1)NAf}$ (MHz)	35	21	0	0	35	35
$\langle T_2\rangle$ (s)	4.9×10^{-7}	4.9×10^{-7}	4.9×10^{-7}	2×10^{-7}	4.9×10^{-7}	2×10^{-7}
σ_{T_2} (s)	0	0	10^{-7}	0.5×10^{-7}	0	0
wt (% of CESR intensity)	71	29	75	25	75	25

[a] Quantities in brackets are the mean values, and σ represents the standard deviation. For each calculation, the equality $T_1 = T_2$ was assumed.

Gaussian distribution, which was applied more conveniently to the quantity $I(I + 1)NAf$ in which the factor $I(I + 1)NA$ is independent of the characteristics of A or B populations. The average contribution $\langle I_{ESR}(B_0)\rangle$ of a given population, A or B, to the CESR spectrum is calculated as follows:

$$\langle I_{ESR}(B_0)\rangle = C \sum_{\text{distribution}} p[I(I+1)NAf] I_{ESR}[B_0, I(I+1)NAf] \quad (10)$$

where C is a normalization factor and $I_{ESR}[B_0, I(I + 1)NAf]$ the CESR intensity given by eq 5 of a particle in population A or B characterized by a value $I(I + 1)NAf$. The term $p[I(I + 1)NAf]$ is the probability of the value $I(I + 1)NAf$ in the Gaussian distribution

$$p[I(I+1)NAf] \propto \exp\{-[I(I+1)NAf - \langle I(I+1)NAf\rangle]^2/(2\sigma_{I(I+1)NAf}{}^2)\} \quad (11)$$

where $\langle I(I + 1)NAf\rangle$ is the mean value and $\sigma_{I(I+1)NAf}$ is the standard deviation. These parameters were adjusted for each population to get the best agreement between calculated and experimental spectra. The resulting values are given in the column CALC 1 of Table 1, and the calculated spectra at $P =$ 25 mW and $T = 4$ K are represented in Figure 4. The contribution of population A, with the highest leakage factor, to the total CESR intensity is 2.5 times that of population B, with the lowest leakage factors. The calculated spectrum under decreasing field sweep fairly reproduces the experimental spectrum and particularly the shoulder and the slope of the left side of the spectrum. However, the calculated spectrum under increasing field sweep is different from the experimental spectrum, since a shoulder is also predicted, which is not observed. Thus, it is necessary to test the second possibility, i.e., a double distribution of electron spin relaxation times T_1 and T_2 (calculation 2). This simulation was performed assuming $T_1 = T_2$, which is usually verified for conduction electron spins in metals. Two Gaussian distributions were chosen for the electron spin relaxation time, and the calculation was performed by summing the CESR intensities corresponding to each population and given by eq 10 in which the distribution of $I(I + 1)NAf$ is replaced by a distribution $p(T_2)$ of T_2. The parameters characterizing the two distributions are given in column CALC 2 of Table 1, and the calculated CESR spectra are shown at the top of Figure 6. The contribution of population A, with the highest T_2 values, to the total CESR intensity is 3 times that of population B, with the lowest T_2 values. It should be pointed out that the ratio of the CESR intensities does not necessarily correspond to the ratio of the number of particles in the populations, since the latter are not characterized by the same CESR saturation factor. With this simulation, the shape of the CESR spectrum under increasing field sweep is now well predicted, since no shoulder appears in the calculated spectrum

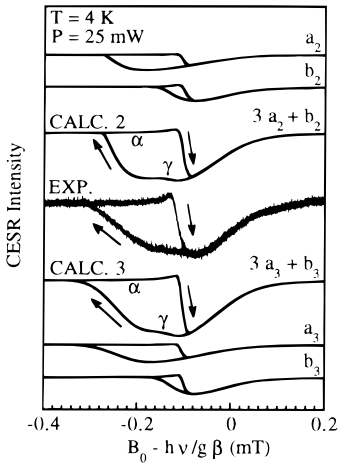

Figure 6. Experimental and calculated BCESR spectra for colloidal lithium particles in irradiated Li_2O at $T = 4$ K and $B_1 = 0.025$ mT ($P = 25$ mW). Calculations 2 and 3 are performed from eqs 2, 3, 5, and 10. Calculation 2 includes two populations of particles, A and B, with Gaussian distributions of the electron spin relaxation times $T_1 = T_2$. Calculation 3 also includes two populations, A and B, of particles with two different values of T_2 and a Gaussian distribution of the leakage factor f. The spectra, a_2 and b_2, a_3 and b_3, represent the individual contributions of each population A and B of particles to the total calculated CESR spectra 2 and 3, respectively. The parameters characterizing the different distributions are given in Table 1.

(Figure 6). However, the slope at the left side of the experimental spectrum under decreasing field sweep is not properly reproduced by the calculation with a double distribution of electron spin relaxation times, since this slope turns out to be too steep in the calculated spectrum. This discrepancy can be qualitatively understood from eq 5, which shows that the CESR intensity is proportional to $T_2{}^3$. As a consequence, only the particles with the highest T_2 values in each population will significantly contribute to the CESR intensity, so the CESR spectrum must be weakly dependent on the width of the distribution.

Therefore, the simulation will have to be improved by combining the effect of a distribution of leakage factor on the slope of the left side of the spectrum under decreasing field sweep and the effect of the existence of two kinds of particles with different electron spin relaxation times T_2. The parameters of this calculation (calculation 3) are given in column CALC 3 of Table 1. A single distribution of $I(I + 1)NAf$ was taken into account with the corresponding parameters $\langle I(I + 1)NAf\rangle = 240$ MHz and $\sigma_{I(I+1)NAf} = 35$ MHz. The value of the electron spin relaxation time T_2 for each kind of particles are, respectively, $\langle T_2\rangle_A = 4.9 \times 10^{-7}$ s and $\langle T_2\rangle_B = 2 \times 10^{-7}$ s. For the sake of simplicity no distribution of the relaxation time T_2 was considered, since this has only a small effect on the CESR line shape. The spectra corresponding to this simulation are given at the bottom of Figure 6. The spectra calculated under both

increasing and decreasing field sweeps appear to be in much better agreement with the experimental spectra than in the two previous calculations. In fact, the existence of two mean electron spin relaxation times should result in two different leakage factors, since the parameters are indirectly connected (eq 9). However, if the overlap between these two distributions of f is large, they can be approximated by a single broad distribution.

The presence of two kinds of particles with different Overhauser shifts was already observed by Gueron and Ryter[12,13] in neutron-irradiated LiF and attributed to a particle-size distribution. Particles with size smaller than the skin depth experienced strong Overhauser shifts, while those larger than the skin depth exhibited no shift because of the nonpenetration of the microwave field. In our case, the particles are smaller than the skin depth ($\delta \approx 1$ μm at X band), since no Dysonian distortion[20] of the unsaturated CESR line is observed. However, a particle-size distribution could also explain the existence of two electron spin relaxation times for lithium particles in Li_2O with particles smaller or larger than the electron mean free path. In the first case, the electrons would undergo frequent collisions with the surface of the particle, inducing a short electron spin relaxation time corresponding to population B. In the second case corresponding to population A with a larger electron spin relaxation time, the surface relaxation process would be much less efficient.

The mean value $\langle I(I + 1)NAf \rangle = 240$ MHz obtained by simulation corresponds to a maximum Overhauser shift $(\Delta B_{ov})_{max} \approx 0.3$ mT calculated at $T = 4$ K from eq 3. This value is much smaller than the value $(\Delta B_{ov})_{max} \approx 0.8$ mT obtained by Ryter for lithium particles in LiF.[12] This means that the leakage factor f (eq 9) of lithium particles in our Li_2O samples is much smaller than in LiF. A small leakage factor f can result from impurities or disorder in the particles, which could increase ν_n' in eq 9 via the quadrupolar relaxation process.

V. Conclusion

We show in this paper that small metallic lithium particles exhibit a bistable conduction electron spin resonance characterized by a "bent" CESR absorption curve, as could be predicted from the general criterion in eq 1. The BCESR spectra of lithium particles could be simulated with the same model as that used for other bistable compounds, β-Ga_2O_3 [5] and InP.[10] This shows that the simple model for BCESR[5] is valid for any kind of material, semiconductor or metal, and that BCESR is a general property of conducting solids with nonzero nuclear spins.

It was also shown that the simulation of the CESR spectra under the bistable Overhauser effect gives semiquantitative information about the distribution of characteristic relaxation times of the particles that cannot be obtained from usual monostable CESR spectra. As a matter of fact, from analysis of the CESR line shapes, we could discriminate between variations of the nuclear relaxation time among the particles affecting the leakage factor and variations of the electron spin relaxation time probably related to a size distribution. However, this hypothesis needs to be confirmed by further experiments on particles with now well-defined characteristics. A quantitative investigation of the effects on BCESR spectra of the size, the purity, and the disorder of the particles that influence both electron and nuclear spin relaxations is necessary.

The elaboration of lithium particles with well-defined characteristics would thus offer possibilities of achieving arrays of coupled bistable systems embedded in an insulating matrix. In such a device, each particle would behave as a bistable system communicating with others via electron tunneling between particles. Hence, new effects such as multistability[21] or enhanced stochastic resonance[2,4] are to be expected.

Acknowledgment. The authors are indebted to J. Perrière and M. Vidal from Groupe de Physique des Solides at University of Paris VI-VII for allowing us to use the van de Graaff accelerator and for their help in the experiments.

References and Notes

(1) Gibbs, H.; Mandel, P.; Peyghambarian, N.; Smith, S. D. *Optical Bistability*; Springer: Berlin, 1986.
(2) Bulsara, A. R.; Gammaitoni, L. *Phys. Today* **1996**, *49*, 39 and references therein.
(3) Benzi, R.; Sutera, S.; Vulpiani, A. *J. Phys. A* **1981**, *14*, L453. Mc Namara, B.; Wiesenfeld, K. *Phys. Rev. A* **1989**, *39*, 4854.
(4) Linder, J. F.; Meadows, B. K.; Ditto, W. L.; Inchiosa, M. E.; Bulsara, A. R. *Phys. Rev. Lett.* **1995**, *75*, 3 and references therein.
(5) Aubay, E.; Gourier, D. *Phys. Rev. B* **1993**, *47*, 15023.
(6) Binet, L.; Gourier, D. *J. Phys. Chem.* **1996**, *100*, 17630.
(7) Overhauser, A. *Phys. Rev.* **1953**, *92*, 411.
(8) Aubay, E.; Gourier, D. *Solid State Commun.* **1993**, *85*, 821.
(9) Solomon, I. *Phys. Rev.* **1959**, *99*, 559.
(10) Binet, L.; Gourier, D. *Phys. Rev. B* **1997**, *56*, 2688.
(11) Taupin, C. *J. Phys. Chem. Solids* **1967**, *28*, 41.
(12) Ryter, C. *Phys. Rev. Lett.* **1960**, *5*, 10.
(13) Gueron, M.; Ryter, C. *Phys. Rev. Lett.* **1959**, *3*, 338.
(14) Vajda, P.; Beuneu, F. *Nucl. Instrum. Methods Phys. Res., Sect. B* **1996**, *116*, 183.
(15) Feher, G.; Isaacson, R. A. *J. Magn. Reson.* **1972**, *7*, 111.
(16) Abragam, A. *Principle of Nuclear Magnetism*; Clarendon Press: Oxford, 1961; p 48.
(17) Anderson, A. G.; Redfield, A. G. *Phys. Rev.* **1959**, *116*, 583.
(18) Stöcklein, W.; Denninger, G. *Mol. Cryst. Liq. Cryst.* **1986**, *136*, 335.
(19) Abragam, A.; Bleaney, B. *Electron Paramagnetic Resonance of Transition Ions*; Dover Publications, Inc.: New York, 1970; p 247.
(20) Feher, G.; Kip, A. F. *Phys. Rev.* **1955**, *98*, 337.
(21) MacKay, R. S.; Sepulchre, J. A. *Physica D* **1995**, *82*, 243.